Macromolecules 1980, *13*, 122-132

Static and Dynamical Properties of Polystyrene in *trans*-Decalin. 4. Osmotic Compressibility, Characteristic Lengths, and Internal and Pseudogel Motions in the Semidilute Regime[‡]

B. Chu* **and T. Nose**[†]

Department of Chemistry, State University of New York at Stony Brook, Long Island, New York 11794.

Received June 28, 1979

ABSTRACT: From measurements of the angular dependence of the absolute scattered intensity of polystyrene ($M_w \sim 1.3 \times 10^7$) in *trans*-decalin as a function of temperature and concentration, we were able to determine the osmotic compressibility $(\partial \pi/\partial C)_{T,P}$ and the composite characteristic length L as a function of reduced temperature difference τ and of scaled concentration C/C^* over extended ranges of the $\tau M^{1/2} - C/C^*$ plane, where $\tau = (T - \Theta)/\Theta$, with Θ being the Θ temperature and C^* being the overlap concentration. Measured single-clipped net signal photoelectron-count time correlation functions were analyzed, using a modified bimodal line width distribution function $G(\Gamma)$ because initial analysis by the histogram method suggested the presence of two peaks in $G(\Gamma)$. Again by varying the scattering angle θ, the temperature, and the concentration, we were able to cover a very broad range in the $K\langle r_g^2\rangle_z^{1/2} - C/C^*$ plane, where K and $\langle r_g^2\rangle_z^{1/2}$ are the magnitude of the momentum transfer vector and the z-average radius of gyration, respectively. We show that the asymptotic regions where simple power laws hold are not easily accessible, that the convergence of the static and dynamical properties to the asymptotic limit depends upon the nature of the parameter, that the boundaries separating the slower translational and molecular motions and the faster local internal motion and pseudogel domains are not sharp, and that at the present time complete separation of different modes in the transition regions is not feasible due to an absence of adequate theory. Our measurements should provide the data for further theoretical treatment in the transition regions of the semidilute region.

Static and dynamical properties of a low molecular weight polystyrene ($M_w = 1.79 \times 10^5$) in *trans*-decalin (a Θ solvent) have been reported.[1,2] In papers 1[1] and 2,[2] we investigated the temperature and the concentration dependence of the osmotic compressibility $(\partial \pi/\partial C)_{T,P}$, the translational diffusion coefficient, the frictional coefficient, and pseudogel motions of entangled polymer coils. By developing a histogram method[3] of correlation function profile analysis, we were able to separate translational motions of polymer coils from the faster gel-like motions of entangled polymer coils in the semidilute region. In paper 3,[4] we have extended our studies to a high molecular weight polystyrene sample ($M_w \sim 1.2 \times 10^7$). By dissolving the high molecular weight polymer in the Θ solvent *trans*-decalin, we have increased the size of the polymer (radius of gyration r_g) substantially, but not so much as to simulate the condition of "infinite" molecular weight in a good solvent where the polymer coil becomes well expanded. The conditions above the Θ temperature correspond to a transition region ($Kr_g \sim 1$) just before the asymptotic limit, where simple power laws hold. By varying the temperature (above the Θ temperature), we can change the polymer coil size and thus vary the Kr_g range. K is the magnitude of the momentum transfer vector. In the dilute solution region,[4] as the polymer characteristic size L ($\equiv r_g$) increases, $KL > 1$ even for small scattering angles, such as $\theta = 30°$. Then, the dynamical structure factor $S(K,t)$ is related to properties of the polymer chain on distances smaller than L which may include hydrodynamic as well as internal motions. We found that the form of $S(K,t)$, as proposed by Dubois-Violette and de Gennes,[5] fitted our experimental time correlation functions exceedingly well, in agreement with the earlier reports of Adam and Delsanti.[6] By remembering that the translational motion of the entire coil becomes more important at smaller scattering angles, we were able to extrapolate to zero scattering angle and to estimate the average size of the hydrodynamic radius ($\bar{r}_h$) of the polymer coil by the method of cumulants.[7] Our measurements in the transition region filled the experimental gap from the Θ region to the asymptotic region, where the temperature and molecular weight dependence of polymer dimension (r_h and r_g) in solution can be represented by the blob theory. The findings were in agreement with those reported by Akcasu and Han,[8] who used all of the literature and some unpublished results, including ours by private communication, of polystyrene in various solvents available at the time. Futhermore, our experiments indicated how the asymptotic limit could be reached. This paper investigates the static and dynamical properties of the same high molecular weight polymer (TSK F-1500 polystyrene) in *trans*-decalin in the semidilute region.

Definitions of Static and Dynamic Properties

In papers 1, 2, and 3, we have expressed and discussed most of the equations used in this article. The purpose of this section is to summarize the definitions of the static and dynamical properties needed in discussing the results so that the article is more self-contained.

1. Static Properties. The osmotic compressibility $(\partial \pi/\partial C)_{T,P}$ is defined by

$$(\partial \pi/\partial C)_{T,P} = H\,(\partial n/\partial C)_{T,P}{}^2 CRT/R_c(0) \qquad (1)$$

where $R_c(0)$ is the excess Rayleigh ratio due to concentration fluctuations at zero scattering angle; H is $4\pi^2n^2/(N_A\lambda_0{}^4)$; n is the refractive index of solution; λ_0 is the wavelength of light in vacuo; R is the gas constant; N_A is the Avogadro number; T is the temperature; P is the pressure; and C is the concentration in g/cm^3 (concentration in g/g will be stated explicitly).

The overlap concentration C^* has an arbitrary definition of the form:

$$C^* = M_w/(N_A\rho_s\langle r_g^2\rangle_z^{3/2}) \qquad (2)$$

where M_w is the weight average molecular weight; ρ_s is the solvent density in g/cm^3; and $\langle r_g^2\rangle_z^{1/2}$ is the z-average radius of gyration.

[‡] Work supported by the National Science Foundation and the U.S. Army Research Office.

[*] Author to whom requests for reprints should be addressed.

[†] On leave of absence from the Department of Polymer Chemistry, Tokyo Institute of Technology, Japan.

0024-9297/80/2213-0122$01.00/0

The characteristic length L can be computed using the relation

$$R_{\mathrm{vv}}(\theta) = R_{\mathrm{vv}}(0)/\left(1 + \frac{L^2}{3}K^2\right) \tag{3}$$

where $K = (4\pi n/\lambda_0) \sin(\theta/2)$. We assume that $L^2 = \langle r_g^2 \rangle_z$ and $C/C^* \ll 1$ for the dilute regime and $L^2 = \xi^2$ and $C/C^* > 1$ for the semidilute regime.

2. Dynamical Properties. The single-clipped photocount autocorrelation function $G_k^{(2)}(t)$ has the form:

$$G_k^{(2)}(t) = A(1 + \beta|g^{(1)}(t)|^2) \tag{4}$$

where A is the background; β is the adjustable parameter; $g^{(1)}(t)$ is the normalized correlation function of scattered electric field; and k is the clipping level.

For a system with multiple decay rates,

$$|g^{(1)}(t)| = \int_0^\infty G(\Gamma) \exp(-\Gamma t)\,\mathrm{d}\Gamma \tag{5}$$

where $G(\Gamma)$ is the normalized distribution of decay rates.

$$\bar{\Gamma} = \int G(\Gamma)\Gamma\,\mathrm{d}\Gamma \tag{6}$$

$$\mu_i = \int (\Gamma - \bar{\Gamma})^i G(\Gamma)\,\mathrm{d}\Gamma \tag{7}$$

Exponent Relations in the Asymptotic Region

1. Static Properties. In dilute solution, the characteristic length L ($\equiv \langle r_g^2 \rangle_z^{1/2}$) can be scaled as

$$\langle r_g^2 \rangle_z^{1/2} \propto N^\nu \tau^r \tag{8}$$

where N is the equivalent number of links in the statistical chain, τ ($\equiv (T - \Theta)/\Theta$) is the reduced temperature distance from the Θ temperature, and $r = 2\nu - 1$.[8]

In the crossover from dilute to semidilute regimes,

$$C^* \propto NL^{-3} \text{ or } N^{1-3\nu}\tau^{-3r} \tag{9}$$

In the semidilute region ($C > C^*$), $L = \xi$ with

$$\xi \propto r_g(C/C^*)^q \text{ or } \tau^p C^q \tag{10}$$

where $q = \nu/(1 - 3\nu)$ and $p = r/(1 - 3\nu)$

$$(\partial\pi/\partial C)_{T,P}/T \propto \frac{1}{N}(C/C^*)^m \text{ or } \tau^n C^m \tag{11}$$

where $m = 1/(3\nu - 1)$ and $n = 3r/(3\nu - 1)$.

2. Dynamical Properties. In semidilute solution,

$$\bar{\Gamma}_f \propto D_g \propto C^\alpha \tag{12}$$

where Γ_f is the line width of the fast mode related mainly to the pseudogel motions, and D_g is the gel diffusion coefficient with $D_g = k_B T/6\pi\eta_0\xi_h$

$$\xi_h \propto D_g^{-1} \propto C^{-\alpha} \tag{13}$$

where ξ_h is the hydrodynamic length in the semidilute region.

By identifying ξ_h with ξ,

$$\alpha = \nu/(3\nu - 1) \tag{14}$$

Experimental Methods

Preparation of solutions, alignment of apparatus, spectrometer calibration, and methods of data analysis have been reported elsewhere.[1-4] Subsequent redeterminations of M_w yielded a value of 1.3×10^7. In this paper, we shall use $M_w = 1.3 \times 10^7$, instead of 1.2×10^7, in our computations. The difference should have no effect in our discussions.

Table I
Osmotic Compressibility (Equation 1) and Characteristic Length (Equation 3) of Polystyrene (TSK F-1500, $M_w \sim 1.3 \times 10^7$) in *trans*-Decalin

	T, °C				
C, wt %	19	20	25	30	40
(a) Osmotic Compressibility $(\partial\pi/\partial C)_{T,P}$ (10^{-4} J g^{-1})					
0.00719				2.22	2.30
0.0106			2.16	2.25	2.39
0.0257		2.16	2.27	2.40	2.69
0.0415		2.26	2.50	2.63	3.21
0.0806		2.34	2.81	3.47	4.10
0.230	2.76	3.23	4.85	6.23	9.47
0.494	2.68	3.64	8.06	11.75	19.64
0.787	2.53	4.24	11.9	19.6	33.3
1.367	3.10	5.50	20.6	35.8	62.2
2.108	4.68	8.98	33.7	58.5	104.1
3.557	10.01	18.55	64.9	108.4	198.0
(b) Characteristic Length L (nm)					
0.00719		123	142	154	170
0.0106		121	139	148	163
0.0257		117	133	142	153
0.0415		114	126	130	137
0.0806		110	118	120	118
0.230	102	95.3	86.8	82.8	73.2
0.494	109	97.1	65.4	58.2	48.8
0.787	106	85.6	51.6	42.9	34.7
1.367	94.4	71.2	41.8	31.3	24.5
2.108	81.4	61.8	30.9	24.2	19.2
3.557	53.4	40.8	23.7	17.4	13.8

Table II
Values of the Overlap Concentration C^* and of the Radius of Gyration at Different Temperatures (TSK F-1500)

T, °C	ρ_s, g/cm^3	$\langle r_g^2 \rangle_z^{1/2}$, nm	C^*, g/g
20	0.8698	123	0.0136
25	0.8659	144	0.00853
30	0.8623	157	0.00671
40	0.8551	175	0.00490

Results and Discussion

1. Static Properties. a. Concentration and Temperature Dependence of Osmotic Compressibility, $(\partial\pi/\partial C)_{T,P}$. The results are summarized in Table Ia. Figure 1a shows plots of the osmotic compressibility as a function of concentration at 19, 20, 25, 30, and 40 °C. At low concentrations in the dilute solution region, the behavior was amplified in Figure 2 of ref 4 where $(\partial\pi/\partial C)/T$ was plotted against concentration up to $C \sim 0.000415$ g/g of solution. There, we already observed an upward curvature at high concentrations, indicating a region of concentration where the virial equation with only the second virial coefficient no longer holds. At temperatures above the Θ temperature (Θ = 20.5 °C), the transition for the osmotic compressibility from the dilute to the semidilute regime is represented essentially by gradual upward increases without sharp identifiable slope changes as shown in Figure 8 of ref 1 for the low molecular weight polystyrene ($M_w = 1.79 \times 10^5$) in *trans*-decalin over the same temperature ranges (20–40 °C). The overlap concentration C^* for the high molecular weight sample ($M_w \sim 1.3 \times 10^7$), as listed in Table II, was reduced to 0.0049 g/g of solution at 40 °C, as compared with $C^* > 0.1$ g/g of solution for the NBS 705 Standard polystyrene ($M_w = 1.79 \times 10^5$) at the same temperature. In other words, for the high molecular weight polymer sample, the dilute solution regime is compressed by a factor of about 30 according to eq 9 and is valid only in the 1×10^{-4} g/g of solution range. The semidilute range where both hydrodynamic and pseudogel modes exist is also more limited. However, on a log scale we can clearly observe regions with $(\partial\pi/\partial C)_{T,P}$ very nearly

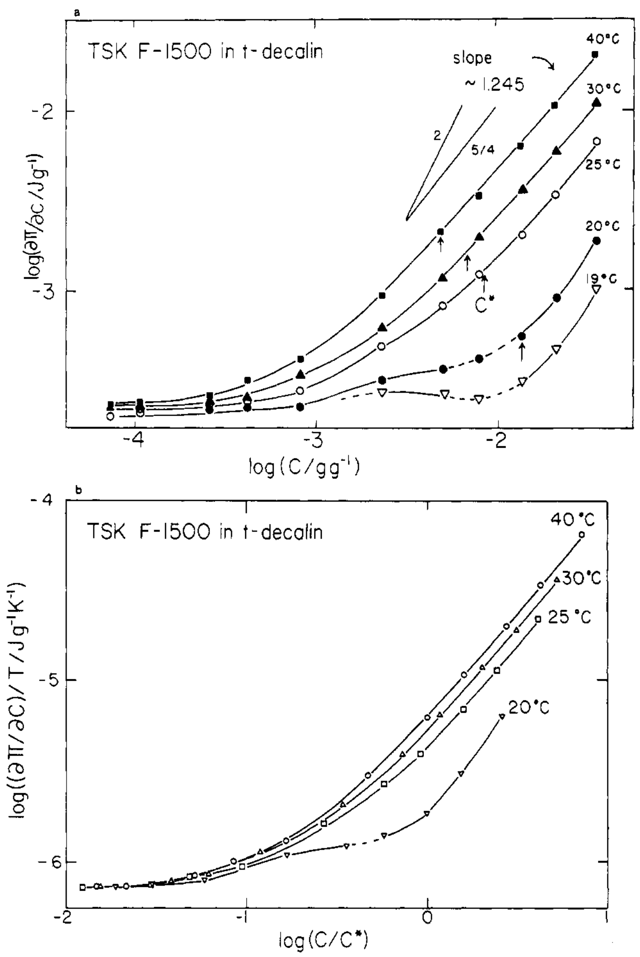

Figure 1. (a) Log-log plots of $(\partial\pi/\partial C)_{T,P}$ vs. C (g/g) for polystyrene (TSK F-1500) in *trans*-decalin. At $T \geq 25$ °C and at $C > C^*$, the slopes are very close to $^5/_4$, predicted for the semidilute region. The depressions at 19 and 20 °C are the results of critical effects. (b) Log-log plots of $(\partial\pi/\partial C)_{T,P}/T$ vs. C/C^* at 20, 25, 30, and 40 °C. According to eq 11, $(\partial\pi/\partial C)_{T,P}/T \propto (1/N)(C/C^*)^m$. Critical effects can easily be observed at 20 °C before the overlap concentration is reached.

proportional to $C^{5/4}$ beyond the overlap concentration C^* at 25, 30, and 40 °C. With concentrations up to about 5 wt % polystyrene in *trans*-decalin, we have not yet reached a slope of 2 in the isotherm plot of $(\partial\pi/\partial C)_{T,P}$ vs. C above the Θ temperature. Near the Θ temperature (at 19 and 20 °C), we also observed the local concentration fluctuations due to critical phenomena. At $C > C^*$, the concentration exponent for $(\partial\pi/\partial C)_{T,P}$ appears to approach a value greater than $^5/_4$. The bump at 19 °C is very prominent. It remains clearly visible at 20 °C but virtually disappears at 25 °C. It is interesting to note that the concentration at which an excess increase in intensity before the dip is observed appears just before the overlap concentration C^* (as defined by eq 2), which is in the neighborhood of the critical solution concentration. We can estimate the critical solution temperature T_c and the critical solution concentration ϕ_c in segment fraction of the high molecular weight polystyrene ($M_w \sim 1.3 \times 10^7$) in *trans*-decalin from the experiments by Nakata et al.[9] as $T_c \sim 19$ °C and $\phi_c \sim 0.014$ g/g of solution. Here the difference between the critical solution temperature and the Θ temperature is small because of the high molecular weight of the polystyrene sample. At 19 °C, we were performing the measurements very near the phase separation temperature for those concentrations in the neighborhood of C^*. In Figure 1b, we have made a log-log plot of $(\partial\pi/\partial C)_{T,P}/T$ vs. C/C^* at 40, 30, 25, and 20 °C. According to eq 11, $(\partial\pi/\partial C)_{T,P}/T$ should scale as $(C/C^*)^m$ in the semidilute regime. We obtained a limiting slope of 1.245 which is in excellent agreement with $\nu = 0.60$. At 20 °C, critical effects take place before the overlap concentration C^*. Scaling in the presence of critical effects is likely to be quite difficult to achieve. However, even in the absence of critical effects, Figure 1b shows that for $(\partial\pi/\partial C)_{T,P}/T$ we have not yet achieved a universal function of scaled concentration C/C^* at temperatures fairly far away from the Θ temperature, i.e., $\tau\Theta$, ~10–20° for a high molecular weight polymer sample dissolved in a Θ solvent. Figure 2a shows plots of log $(\partial\pi/\partial C)_{T,P}$ vs. temperature at different concentrations. At low concentrations in the dilute solution region, such as $C = 0.72 \times 10^{-4}$ g/g of solution and 1.06×10^{-4} g/g of solution, we note that at $T > \Theta$, the second virial coefficient A_2 of the equation $(\partial\pi/\partial C)_{T,P}/RT = 1/M_w + 2A_2C$ is positive. The slope increases with increasing concentration. The curves in the dilute solution region should cross over at the Θ temperature as A_2 then becomes negative. At higher concentrations, the upward curvature as shown in Figure 2 of ref 4 dominates. Therefore, the crossover is no longer observed. At $C \gtrsim C^*$, we expect $(\partial\pi/\partial C)_{T,P}/T \propto \tau^n$, as shown in Figure 2b, where $n = 0.75$. If we take $\nu = 0.6$ and $n = 3r/(3\nu - 1)$, $r = 0.2$. In Figure 5b of ref 4 we observed that for the high molecular weight polymer sample dissolved in a Θ solvent and at $\Theta\tau \sim 20$ °C, the radius of gyration was still not quite large enough for it to reach the asymptotic region where $r = 0.2$. Yet in the $(\partial\pi/\partial C)_{T,P}/T$ term, we have evidently achieved a value of 0.75 for n, as predicted by the scaling theory for the semidilute regime. It appears that the range of the asymptotic region where simple power laws hold depends upon the nature of the parameters of interest. We knew that the rate of convergence to the asymptotic limit ($N \rightarrow \infty$) is faster for static properties than for dynamical properties.[10] We now show that among the static properties, $(\partial\pi/\partial C)_{T,P}$ approaches $\tau^{0.75}$ earlier than $\langle r_g^2\rangle_z^{1/2}$ approaches $\tau^{0.2}$ under our experimental conditions.

The critical effects can best be visualized by plotting $(\partial\pi/\partial C)_{T,P}^{-1}$ vs. C (g/g). For a binary fluid mixture, $(\partial\pi/\partial C)_{T,P} = 0$ at the critical mixing point. Therefore, in a plot of $(\partial\pi/\partial C)^{-1}$ vs. C, as shown in Figure 3, we can observe the critical effects implying infinite scattered intensity at the critical mixing point. The same effect can be observed if we make a plot of isotherms of L vs. C. Near the critical mixing point, the range of correlations increases, and we should observe an anomalous increase in L. For the high molecular weight polymer which has a sufficiently broad molecular weight distribution, it is likely that the polymer composition at which maximum phase separation temperature occurs is located at a lower concentration than the critical solution concentration. We have noted that near the maximum phase separation temperature the overlap concentration C^* occurs only at a slightly higher concentration than the observed critical effect. The coincidence may not be accidental and suggests a close connection between the overlap concentration C^* and the critical solution concentration.

b. Concentration and Temperature Dependence of Characteristic Length L. The results are summarized in Table Ib. Figure 4a shows a log–log plot of L vs. C at different temperatures. As the radius of gyration increases with increasing temperature, C^* decreases with increasing temperature. However, at higher concentrations, L decreases with increasing temperature. The crossover behavior in the temperature dependence of the characteristic length occurs at $C < C^*$. In the semidilute region, $L \equiv \xi$

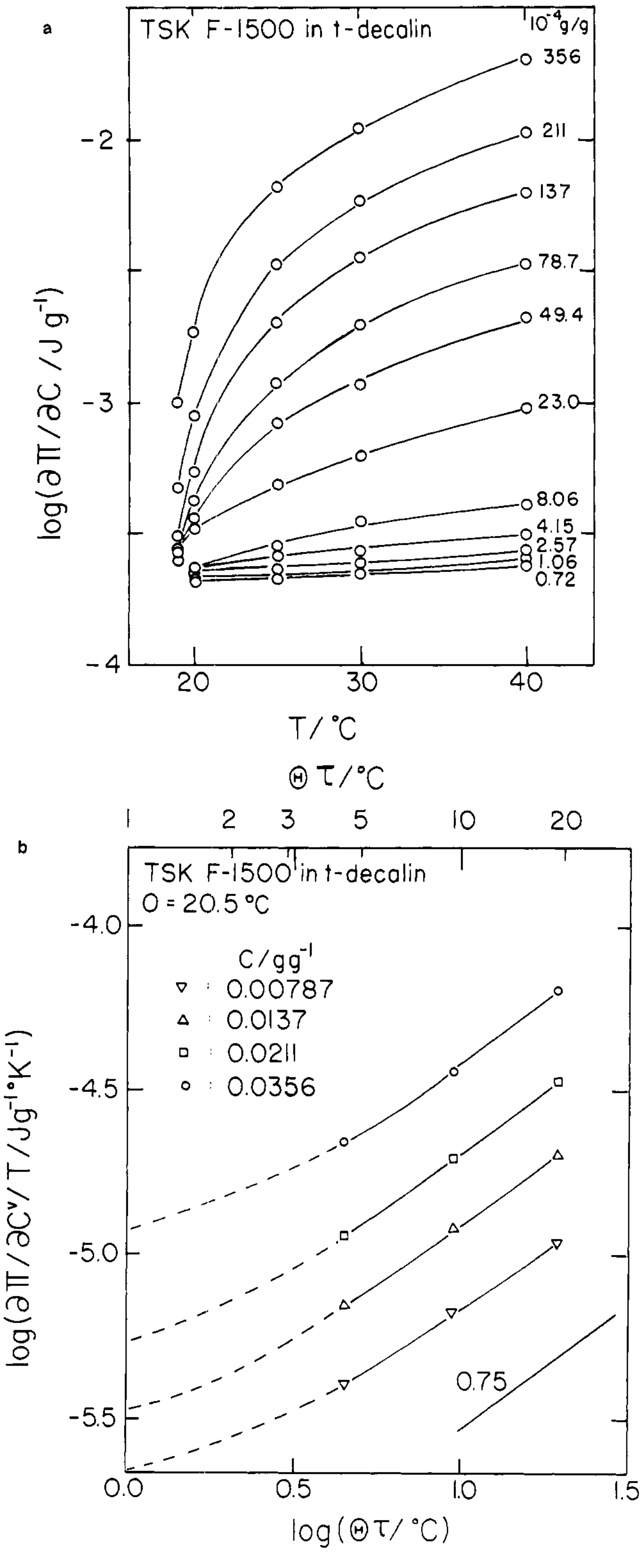

Figure 2. (a) Plots of log $(\partial\pi/\partial C)_{T,P}$ vs. temperature at different concentrations from the dilute to the semidilute regimes. (b) Log-log plots of $(\partial\pi/\partial C)_{T,P}/T$ vs. Θ τ. According to eq 11, $n = 3r/(3\nu - 1) = 0.75$ for $\nu = 0.6$ and $r = 0.2$.

$\propto C^q$, with $q = \nu/(1 - 3\nu)$. As $C^* = 0.0049$ g/g and 0.0067 g/g at 40 and 30 °C, respectively, we obtained a limiting slope for q of -0.63 ± 0.01 and -0.61 ± 0.01 at those two respective temperatures. The important point is that, in the concentration range of our investigation, $|q|$ increases with increasing temperature. We predict that as our polymer solution has not yet reached the asymptotic region which is valid for very large polymer coils in a good solvent, the value of $|q|$ should approach $^3/_4$ if we were to increase the temperature in order to expand the polymer coils and to move the system further into the good solvent regime. According to eq 10, we have $L/\langle r_g^2\rangle_z^{1/2} \propto (C/C^*)^q$ in the semidilute region with $q = \nu/(1 - 3\nu) = {}^3/_4$ for $\nu = 0.6$. Thus, in a log-log plot of $L/\langle r_g^2\rangle_z^{1/2}$ vs. (C/C^*), the reduced quantity $L/\langle r_g^2\rangle_z^{1/2}$ should scale with C/C^* for isotherms of the polymer solution in the asymptotic region. As our system is still in the transition region, we do not expect presentation of a universal curve in such a plot. Furthermore, the determination of L in the transition region according to eq 3 is only approximate, as the scattering curve contains information on $\langle r_g^2\rangle_z$ as well as ξ^2. Here we will refer to the transition region being the concentration where the virial equation with only the second virial coefficient no longer holds but $C < C^*$ as defined by eq 2. Figure 4b shows that, with increasing temperatures, the isotherms tend to bunch closer together. It should be noted that our system of polystyrene with $M_w \sim 1.3 \times 10^7$ in a Θ solvent (*trans*-decalin) has still not yet met the very stringent conditions of the asymptotic limit at 10–20 °C above the Θ temperature. Further theoretical development in the transition region which covers most of the actual experimental conditions should be very useful.

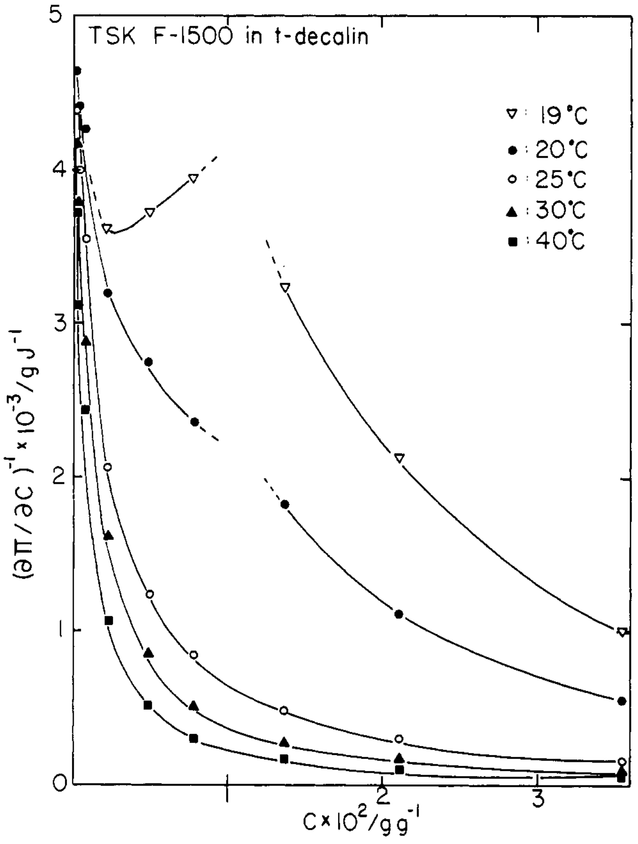

Figure 3. Plots of $(\partial\pi/\partial C)_{T,P}^{-1}$ vs. C (g/g) at different temperatures. For a binary fluid mixture, $(\partial\pi/\partial C)_{T,P} = 0$ at the critical mixing point. $C^* = 0.0136$ g/g of solution at 20 °C.

The temperature dependence of the characteristic length L has the form $L \propto \tau^r$ in the dilute region and $L \propto \tau^p$ with $p = r/(1 - 3\nu)$ in the semidilute region. In the asymptotic limit, for $r = 0.2$ and $\nu = 0.6$, $p = -0.25$. Figure 5a shows plots of log L vs. temperature at different concentrations. The solid circles denote the values of the characteristic length L extrapolated to zero concentration or $\langle r_g^2\rangle_z^{1/2} = \lim_{C\to 0} L$. In the dilute solution region, L is similar to $\langle r_g^2\rangle_z^{*1/2}$ which increases with increasing temperature as r is positive. The polymer coil appears to contract faster below the Θ temperature. Crossover occurs at around 0.2

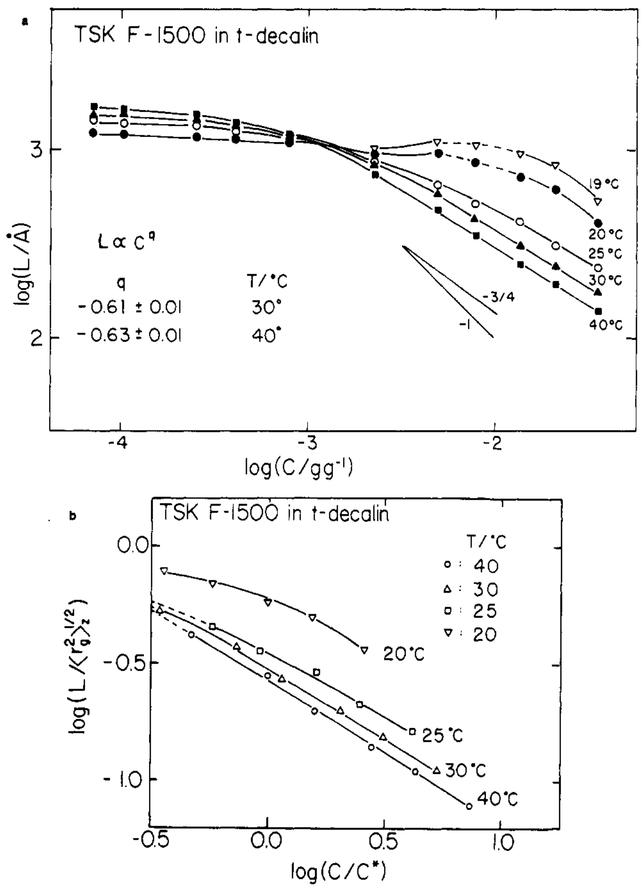

Figure 4. (a) Log-log plots of L vs. C (g/g) at different temperatures. In the semidilute regime, $L \propto C^q$, with $q = \nu/(1-3\nu) = -3/4$ for $\nu = 0.6$. At 40 °C, log (C^* (g/g of solution)) = −2.31. (b) Log-log plot of $L/\langle r_g^2\rangle_z^{1/2}$ vs. C/C^* at different temperatures.

wt % polystyrene as has been shown also in Figure 4a. At higher concentrations, L corresponding to the characteristic length between knots decreases with increasing temperature. Values of L at high concentrations and high temperatures can be quite small, about the order of 15 nm in our studies. Figure 5b shows log-log plots of L^2 vs. $\Theta\tau$ in the semidilute region. We obtained $p \sim -0.35$, in any case larger in magnitude than the theoretical predictions of −0.25. Over the concentration and temperature ranges of our investigation, we got $r < 0.2$ in the dilute solution region. Consequently, with $p = r/(1-3\nu)$, $|p|$ should be less than 0.25. This discrepancy with theory is related to the breakdown of the scaling equation for L (eq 10) in our experimental range, as shown in Figure 4b.

When we determine the characteristic length ξ which is related to the average distance between adjacent contact points and the radius of gyration of the entire polymer coil, we have used eq 3 for both effects, regardless of the concentration ranges. In fact, there is a very large transition region in concentration where we can observe both contributions.[1,2] Therefore, in the transition range, the characteristic length L is an apparent parameter which is a composite of coil size and adjacent contact point characteristic length. Without a proper separation of the effects, it would be too optimistic to expect eq 10 to remain valid at concentrations near C^*. However, we can still provide meaningful discussions on a qualitative basis. Figure 6 shows plots of isotherms of the characteristic length L as a function of concentration. At 25, 30, and 40 °C, the temperatures are sufficiently far away from the critical temperature that the long-range order of critical fluctuations is negligibly small. Near the maximum phase separation temperature which can be slightly higher than the critical solution temperature for a polydisperse polystyrene sample dissolved in *trans*-decalin, we observed an anomaly located at a slightly lower concentration than that determined in an intensity plot as shown in Figure 3. This behavior again illustrates the fact that L is a composite quantity representing a mixture of weighted characteristic lengths.

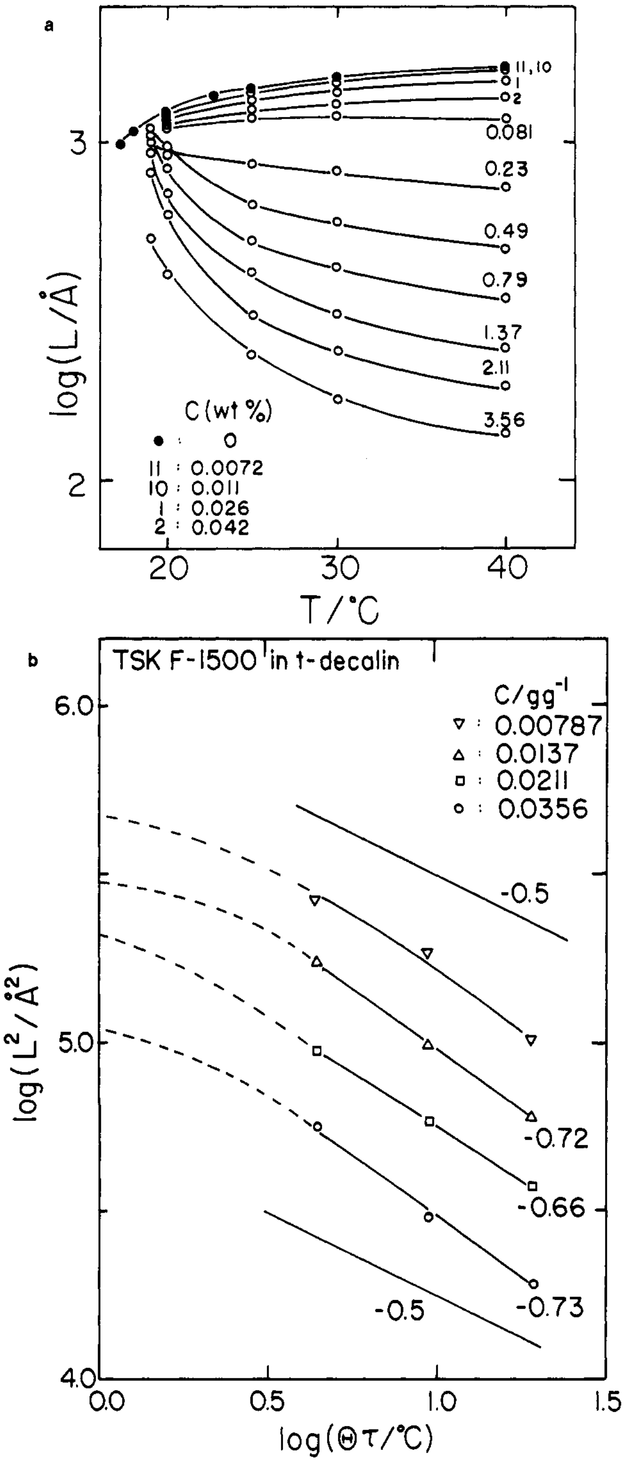

Figure 5. (a) Plots of L vs. temperature at different concentrations. Solid circles denote values of L extrapolated to zero concentration: $L = \langle r_g^2\rangle_z^{1/2}$. (b) Log-log plots of L^2 vs. $\Theta\tau$ in the semidilute region.

By using the high molecular weight polystyrene sample (TSK F-1500, $M_w \sim 1.3 \times 10^7$), we have extended the ranges of our studies in the temperature composition diagram by a very large margin when compared with pre-

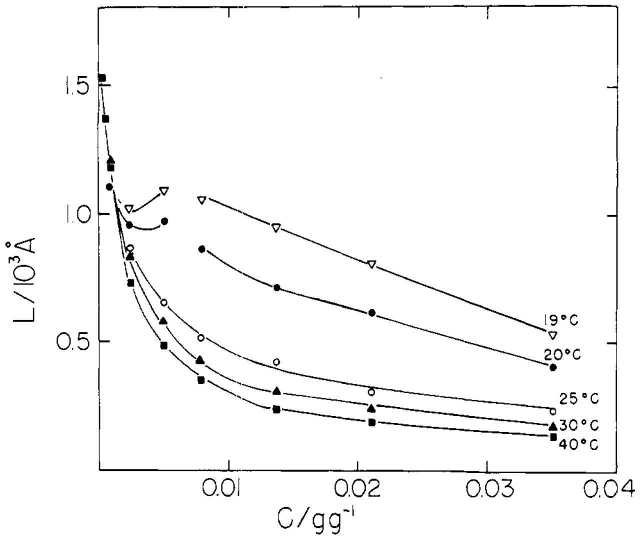

Figure 6. Plots of isotherms of L vs. C (g/g). The anomaly occurs near the critical mixing point where the critical solution temperature is estimated to be about 19 °C.

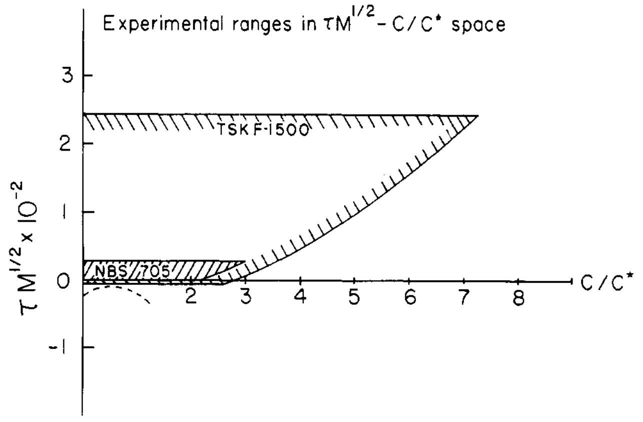

Figure 7. Schematic diagram of experimental ranges of TSK F-1500 and NBS 705 Standard[1,2] polystyrene samples in the $\tau M^{1/2} - C/C^*$ plane.

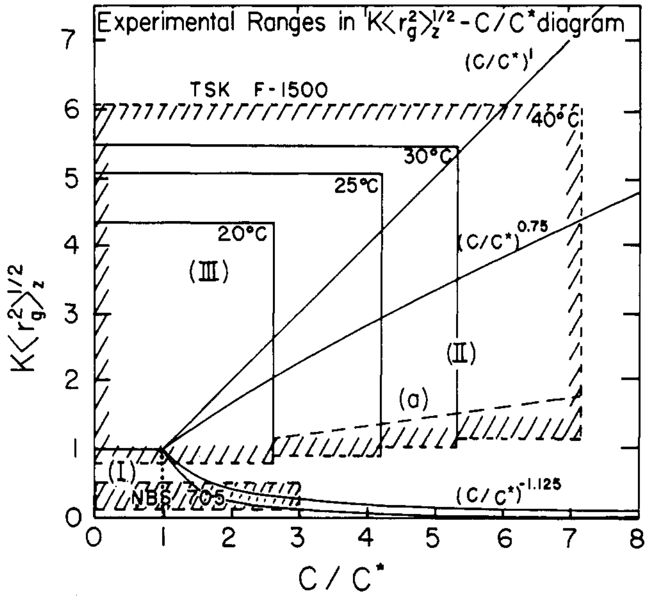

Figure 8. Schematic diagram of experimental ranges of TSK F-1500 and NBS 705 Standard[1,2] polystyrene samples in the $K\langle r_g^2\rangle_z^{1/2} - C/C^*$ plane: I, $KL \ll 1$, dilute solutions; II, pseudogel domain; and III, $KL \gg 1$, internal motions dominate. The curve below $K_{\min}L = (C/C^*)^{-1.125}$ corresponds to $KL = (C/C^*)^{-2}$. Curve a represents the changes in the $K\langle r_g^2\rangle_z^{1/2} - C/C^*$ plane for Figure 14 at $C = 0.0356$ g/g of solution, $\theta = 30°$, and temperatures from 20 to 40 °C.

vious reported results of a low molecular weight polystyrene sample (NBS 705 Standard, $M_w \simeq 1.79 \times 10^5$) in *trans*-decalin. Figure 7 shows a schematic diagram of the experimental ranges which we have studied in the $\tau M^{1/2} - C/C^*$ plane. The broken line represents an estimated coexistence curve of the TSK F-1500 polystyrene in *trans*-decalin based on earlier measurements of lower molecular weight polystyrene samples by Kuwahara and his co-workers.[9]

2. Dynamical Properties: Internal and Pseudogel Motions. a. Line Width Analysis. In dilute solutions, we have access to the translational diffusion coefficient of the entire polymer coil at $Kr_g \ll 1$, whereas at $KL \gg 1$, the dynamical structure factor is related to internal motions of the polymer chain. However, the transition from measurements of the translational motion of the entire coil to local motions is not sharp, as shown in Figures 7–9 of ref 4. We have indicated the domain for the dilute solution region as (I) with $K_{\max}\langle r_g^2\rangle_z^{1/2} = 1$ at $C/C^* < 1$. At $C/C^* > 1$, $K_{\max} = \langle r_g^2\rangle_z^{1/2}(C/C^*)^{0.75}$, which suggests that in the semidilute region we see essentially the gel picture with $D_g \propto C^\alpha$ and $\alpha = \nu/(3\nu - 1) = 0.75$ for $\nu = 0.6$. Again we should emphasize that the transition from the pseudogel region to the domain where internal motions dominate is not sharp. The gel picture has a lower limit with $K \geq K_{\min} = \langle r_g^2\rangle_z^{1/2}(C/C^*)^{-1.125}$ for $\nu = 0.6$. In Figure 8, which is equivalent to Figure 1 of the second paper of ref 6, we have presented the experimental ranges of our investigations for both the NBS 705 Standard polystyrene[1,2] ($M_w = 1.79 \times 10^5$) in *trans*-decalin and the TSK F-1500 polystyrene ($M_w \sim 1.3 \times 10^7$) in *trans*-decalin in the $K\langle r_g^2\rangle_z^{1/2} - C/C^*$ plane. By using a Θ solvent, we were able to vary our experimental ranges by changing the temperature. Furthermore, we have added $K_{\min}\langle r_g^2\rangle_z^{1/2} = (C/C^*)^{2\nu-3/2(3\nu-1)} = (C/C^*)^{-2}$ and $K_{\max}\langle r_g^2\rangle_z^{1/2} = (C/C^*)^{\nu(3\nu-1)} = (C/C^*)^1$ for $\nu = {}^1/_2$ in a Θ solvent.

In the pseudogel domain (II), Adam and Delsanti[6] observed that the dynamical structure factor $S(K,t)$ could be represented by a single exponential function of time. Furthermore, the inverse characteristic time of $S(K,t)$ was proportional to K^2 with D_g $(= (1/\tau)/K^2)$ determined to within 5%. According to eq 12 and 13, they obtained $\alpha = 0.67 \pm 0.02$ instead of 0.75, which is the theoretical prediction. In view of the fact that all changes from (I) to (II), (I) to (III), and (II) to (III) involve fairly broad transition regions, we shall proceed with our data analysis in the semidilute region without fitting a single exponential function of time to the dynamical structure factor. By using a histogram method of correlation function profile analysis, we observed a bimodal distribution function of line width in the semidilute region. As the histogram method does not require an a priori assumption on the form of the distribution function, it appears that the dynamical structure factor has a composite time behavior for solutions in all the transition regions. Here we refer to a mixing of gel-like motions with local motions of the polymer coil and other overlaps. Indeed, a major portion of the semidilute region exhibits a composite of translational and gel-like time behavior for $K\langle r_g^2\rangle_z^{1/2} < 1$ and $C/C^* \gtrsim 1$, whereas the composite characteristic time changes to internal and pseudogel motions for $K\langle r_g^2\rangle_z^{1/2} > 1$ and $C/C^* \gtrsim 1$.

In the histogram method, although we can obtain an approximate form of $G(\Gamma)$, the bimodal distribution requires an extra amount of computer time for data analysis. Furthermore, the relatively narrow line width distribution

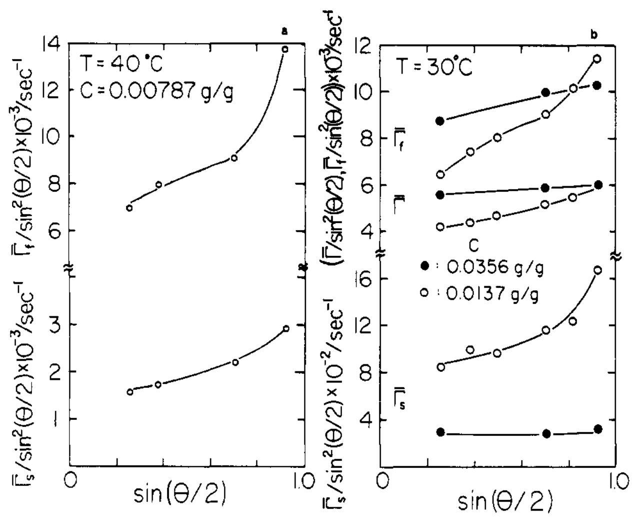

Figure 9. (a) Plots of $\bar{\Gamma}_s/\sin^2(\theta/2)$, $\bar{\Gamma}_f/\sin^2(\theta/2)$ vs. $\sin(\theta/2)$; $C/C^* = 1.61$; $K\langle r_g^2\rangle_z^{1/2}$ varied from 1.71 to 6.09; $C = 0.00787$ g/g of solution. (b) Plots of $\bar{\Gamma}_s/\sin^2(\theta/2)$, $\bar{\Gamma}/\sin^2(\theta/2)$, $\bar{\Gamma}_f/\sin^2(\theta/2)$ vs. $\sin(\theta/2)$ at $C = 0.0137$ g/g of solution ($C/C^* = 2.04$) and 0.0356 g/g of solution ($C/C^* = 5.31$).

of the slower component as well as the close vicinity of the two peaks makes the fitting of such experimental curves by the least-squares histogram method very difficult. Consequently, we have used a simplified *approximate* expression

$$A\beta|g^{(1)}(\tau)|^2 = A\beta[A_f \exp(-\bar{\Gamma}_f\tau + \mu_{2f}\tau^2/2) + A_s \exp(-\bar{\Gamma}_s\tau)]^2 \quad (15)$$

for analyzing the data of TSK F-1500 in *trans*-decalin in the semidilute region. The constants A_f and A_s represent the strength of the scattered intensity at a fixed concentration, temperature, and scattering angle. The subscripts f and s denote the fast and slow motions. In fact, we have approximated $G(\Gamma)$ by

$$G(\Gamma) = G_s'(\Gamma) + G_f'(\Gamma) = A_s\delta(\Gamma - \bar{\Gamma}_s) + A_f \exp[-(\Gamma - \bar{\Gamma}_f)^2/2\mu_{2f}] \quad (16)$$

Figure 9 shows a plot of $\bar{\Gamma}_s/\sin^2(\theta/2)$ vs. $\sin(\theta/2)$ and $\bar{\Gamma}_f/\sin^2(\theta/2)$ vs. $\sin(\theta/2)$ at 40 °C and $C = 0.00787$ g/g of solution. According to Table I, we have $\langle r_g^2\rangle_z^{1/2} = 1.75 \times 10^{-5}$ cm and $C^* = 0.0049$ g/g of solution. Thus, we have covered the $K\langle r_g^2\rangle_z^{1/2}$ range from 1.71 to 6.09 at $C/C^* = 1.61$. At large scattering angles, the characteristic time is related mainly to local internal motions, as shown in Figure 8. In fact, C/C^* is only slightly greater than 1, and we may attempt to utilize the dynamical structure factor proposed by Dubois-Violette and de Gennes[5] as we have discussed in paper 3[4] for the dilute solution region. However, at $K\langle r_g^2\rangle_z^{1/2} \sim 1.5$ and $C/C^* \sim 1.5$ the dynamical structure factor must contain information on the time behavior of local internal motions as well as pseudogel motions. Then, we have to make an appropriate accommodation in our data analysis. The histogram method revealed a bimodal line width distribution, and we used eq 15 and 16 to provide a semiquantitative representation on the strength and magnitude of the characteristic time associated with translational, pseudogel, and local internal motions. $\bar{\Gamma}_s$ is related to the translational motion of the polymer coil. By extrapolating $\bar{\Gamma}_s/\sin^2(\theta/2)$ to zero scattering angle, we can compute a limiting diffusion coefficient $\bar{D}_s$ ($\equiv \lim_{K\to0}\bar{\Gamma}_s/K^2$) $\sim 1 \times 10^{-8}$ cm^2/s, which corresponds to an effective hydrodynamic radius of about 1×10^2 nm, roughly 10% larger than $\bar{r}_h$ at 40 °C.[4] As some entanglement of the polymer coil should increase the effective hydrodynamic size, this result is surprisingly good in view of the large changes in the macroscopic viscosity which have taken place from solvent viscosity to polymer solution viscosity at 0.00787 g/g of solution.

The apparent slope in Figure 9 for the $\bar{\Gamma}_s/\sin^2(\theta/2)$ vs. $\sin(\theta/2)$ plot can be attributed to incomplete separation of our characteristic times, using the approximate expression of eq 15, and/or to the local slow motions accompanied with disentanglement at high scattering angles. In the $\bar{\Gamma}_f/\sin^2(\theta/2)$ vs. $\sin(\theta/2)$ plot, we have noted a sharp upward curvature at higher scattering angles and $C/C^* \sim 1.6$. Again the initial slope is the result of mixing the pseudogel motions with the local internal motions. At $K\langle r_g^2\rangle_z^{1/2} \sim 1.5$, even though Figure 8 suggests that we are already in the internal motion domain, we see both pseudogel motions and local internal motions. The upward slope consists of a weighted average of the composite characteristic times related to pseudogel and local internal motions. At large scattering angles where $K\langle r_g^2\rangle_z^{1/2} \sim 5$ the local internal motion finally dominates. Then we have a fairly sharp upward curvature, implying that the inverse characteristic time is approaching a K^3 dependence in domain (III). Both local internal motions and pseudogel motions are faster than the translational motion of polymer chains.

Figure 9b shows plots of $\bar{\Gamma}_s/\sin^2(\theta/2)$, $\bar{\Gamma}/\sin^2(\theta/2)$, and $\bar{\Gamma}_f/\sin^2(\theta/2)$ vs. $\sin(\theta/2)$ at 30 °C and $C = 0.0137$ and 0.0356 g/g of solution, respectively. In the $K\langle r_g^2\rangle_z^{1/2} - C/C^*$ diagram, the variation corresponds to two paths: one at $C/C^* = 2.04$ with $K\langle r_g^2\rangle_z^{1/2}$ varying from 1.54 to 5.49; the other at $C/C^* = 5.31$ with the same $K\langle r_g^2\rangle_z^{1/2}$ range. At low scattering angles ($K\langle r_g^2\rangle_z^{1/2} \sim 1.5$), $\bar{\Gamma}_s$ decreases with increasing concentration because the overall translational motions of the entire coil including entanglement with other coils slow down. In other words, the effective hydrodynamic size increases with increasing concentration. At $K\langle r_g^2\rangle_z^{1/2} \sim 1.5$, $\bar{\Gamma}_f$ increases with increasing concentration because, according to Figure 8, as we move from $C/C^* = 2.04$ to 5.31, we observe more pseudogel motions which are faster than the local internal motions. At $C = 0.0356$ g/g of solution, $\bar{\Gamma}_s/\sin^2(\theta/2)$, $\bar{\Gamma}/\sin^2(\theta/2)$, and $\bar{\Gamma}_f/\sin^2(\theta/2)$ remain relatively constant as a function of θ over the entire range of our investigation, whereas at $C = 0.0137$ g/g of solution, $\bar{\Gamma}_s/\sin^2(\theta/2)$ has an apparent increase at large scattering angles probably because of the increase contributed by the local internal characteristic time of disentanglement motions or because of the incomplete separation of the fast and the slow motions. It should be interesting to note that at $C = 0.0137$ g/g of solution or $C/C^* = 2.04$, we can observe an upward curvature in the $\bar{\Gamma}_f/\sin^2(\theta/2)$ vs. $\sin(\theta/2)$ plot, as shown in Figure 9b. A similar behavior is exhibited in Figure 9a for $C = 0.00787$ g/g of solution. However, for $C = 0.0356$ g/g of solution, no upward curvature is observed. We believe that at $C = 0.0356$ g/g of solution or $C/C^* = 5.31$, $\bar{\Gamma}_f/\sin^2(\theta/2)$ should eventually also exhibit an upward curvature at a higher value of $K\langle r_g^2\rangle_z^{1/2}$. The upward curvature is delayed because over the angular range of our investigation, the pseudogel motion dominates and the local internal motions have not yet contributed sufficiently strongly to produce a K^3 dependence for $\bar{\Gamma}_f$, which represents a composite characteristic time for pseudogel and local internal motions. In Figure 9b, we have also plotted $\bar{\Gamma}/\sin^2(\theta/2)$ vs. $\sin(\theta/2)$ to indicate that we can learn little from the unresolved overall line width.

Figure 10 shows a plot of $\bar{\Gamma}_f$, $\bar{\Gamma}_s$, and $\bar{\Gamma}$ vs. concentration at 30 °C and $K\langle r_g^2\rangle_z^{1/2} \sim 1.5$ for TSK F-1500 in *trans*-decalin. The dotted lines denote the values at low concentrations ($C/C^* < 1$) where we fitted the dynamical

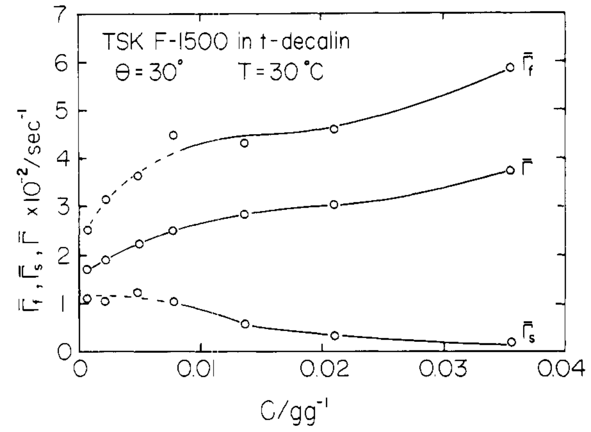

Figure 10. Plot of $\bar{\Gamma}_f$, $\bar{\Gamma}_s$, and $\bar{\Gamma}$ vs. concentration (g/g) at 30 °C and $\theta = 30°$ for TSK F-1500 in *trans*-decalin.

structure factor using our approximate eq 15 while we should have used the nonexponential form which has taken into account hydrodynamic interactions between segments. However, we were able to estimate the correct value of $\bar{\Gamma}_s$ ($= \bar{D}_s K^2$) which yields a hydrodynamic radius $\bar{r}_h$ of 8.6 × 10 nm at 30 °C in very good agreement with the results of ref 4. At higher concentrations, $\bar{\Gamma}_s$ eventually decreases because the polymer coils are all entangled together in the semidilute region. For $\bar{\Gamma}_f$, which is a composite line width, we first see mainly the time behavior of internal motions at low concentrations ($C/C^* < 1$) in Figure 10. The pseudogel characteristic increases with increasing concentration, as shown schematically in Figure 8. Therefore, $\bar{\Gamma}_f$ increases with concentration because of the faster pseudogel motions. In the semidilute region, at $C/C^* > 1$, we have plotted $\bar{\Gamma}_f$ vs. C, as shown in Figure 11a. At 40 °C where the polymer coil is more expanded, $\bar{\Gamma}_f \sim C^\alpha$ with $\alpha = 0.43$. According to eq 12 and 14, $\bar{\Gamma}_f \sim D_g \sim C^\alpha$ with $\alpha = \nu/(3\nu - 1) = 0.75$ for $\nu = 0.6$ and $\alpha = 1$ for $\nu = {}^1/_2$. The difficulty here is that our $\bar{\Gamma}_f$ cannot be identified with $\bar{D}_g K^2$, as it is a composite line width which includes some local internal motions.

Figure 11b shows a similar log-log plot of $\bar{\Gamma}_s$ vs. concentration in the semidilute region. As we have mentioned previously, the slow translational motions can be related to the entire polymer coil diffusion at infinite dilution. In the semidilute region, $\bar{\Gamma}_s$ is related to translational motions of entangled polymer coils, including a finite lifetime T_r of the polymer network[5] with

$$T_r = \frac{6\pi\eta_0}{k_B T}\langle r_g^{\,2}\rangle_z^{\,3/2}(C/C^*)^{3(1-\nu)/(3\nu-1)} \qquad (17)$$

where $3(1 - \nu)/(3\nu - 1) = -1.5$ for $\nu = 0.6$ and D (self-diffusion) $\sim r_g^{\,2}(C)/T_r \sim C^{-1.75}$.[11] We did observe $\bar{\Gamma}_s \sim C^{-1}$ at 30 °C and $\theta = 30°$, as suggested by Figure 11b. Again, we do not expect that $\bar{\Gamma}_s$ can follow the asymptotic behavior because our apparent $\bar{\Gamma}_s$ at $\theta = 30°$ contains some contribution of the faster modes, especially at higher concentrations. Here, we refer to the faster modes in a general sense because the contributions include both fast motions due to incomplete separation by means of eq 15 and the faster local modes of slow motions of chain segments (probably of many chains), since the condition $K\langle r_g^{\,2}\rangle_z^{\,1/2} \ll 1$ is not satisfied. Then the apparent slope will be shallower than the theory predicts, as we have shown in Figure 11b. Figure 11c shows log-log plots of $\bar{\Gamma}$ vs. C (g/g) at $\theta = 30°$, $C/C^* \gtrsim 1$, and different temperatures. In the unresolved line width $\bar{\Gamma}$, we note an increase of $\bar{\Gamma}$ with respect to concentration at 40 °C where $\bar{\Gamma} \sim C^{0.41}$, but $\bar{\Gamma}$ is virtually independent of concentration at 20 °C. At 40 °C, the faster modes dominate and thus $A_f > A_s$ at $\theta = 30°$. $\bar{\Gamma}$ behaves more like $\bar{\Gamma}_f$. At 20 °C, the slow (translational and disentanglement) and the fast (internal and pseudogel) modes are of comparable magnitude. While $\bar{\Gamma}_f$ increases with increasing concentration, $\bar{\Gamma}_s$ decreases with increasing concentration. Thus, over the short concentration range of our studies, $\bar{\Gamma}$ is virtually independent of concentration, as shown in Figure 11c. The fact that $\bar{\Gamma}$ behaves more like $\bar{\Gamma}_f$ at 40 °C than $\bar{\Gamma}_f$ at 20 °C can be illustrated from a log-log plot of $\bar{\Gamma}_s$, $\bar{\Gamma}_f$, and $\bar{\Gamma}$ as a function of temperature. At 20 °C, $\bar{\Gamma}$ is almost halfway between $\bar{\Gamma}_s$ and $\bar{\Gamma}_f$, while at 40 °C, $\bar{\Gamma} \sim \bar{\Gamma}_f$, as shown in Figure 12.

In paper 3,[4] we have examined the relationship between the hydrodynamic radius and the radius of gyration in the dilute solution region where $\bar{r}_h \propto \langle r_g^{\,2}\rangle_z^{\,1/2}$ above the Θ

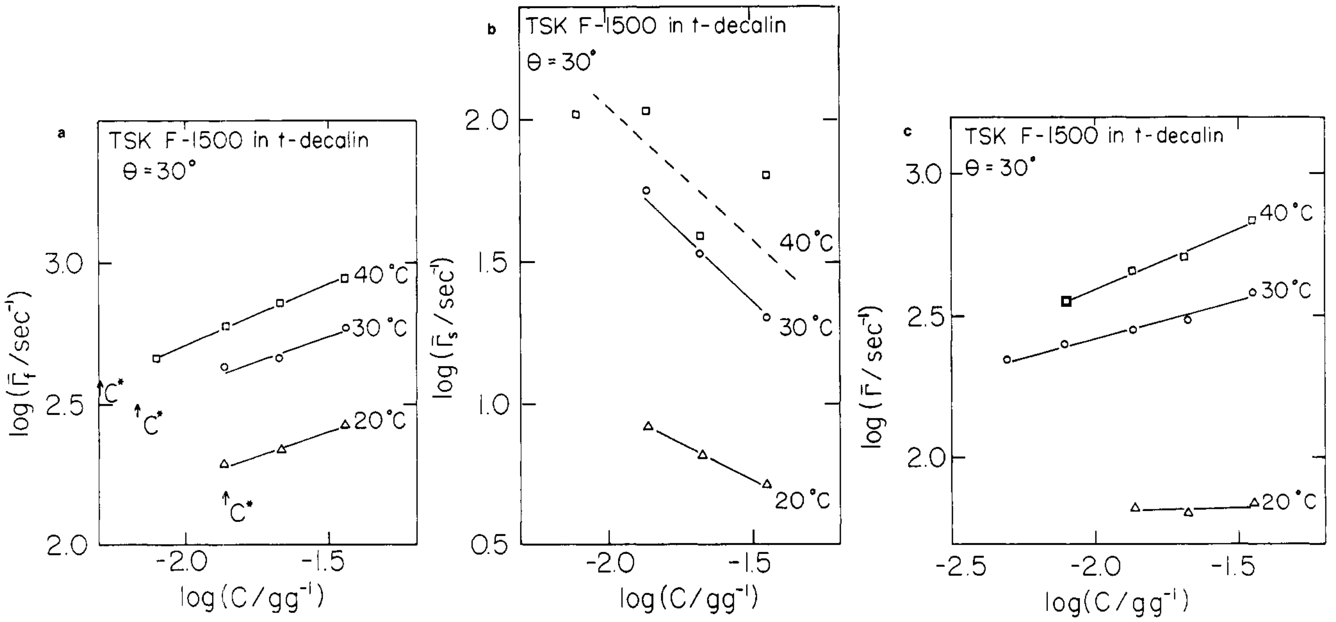

Figure 11. (a) Log-log plots of $\bar{\Gamma}_f$ vs. C (g/g) at $K\langle r_g^{\,2}\rangle_z^{\,1/2} \sim 1.5$ ($\theta = 30°$), $C/C^* > 1$, and different temperatures. (b) Log-log plots of $\bar{\Gamma}_s$ vs. C (g/g) at $\theta = 30°$, $C/C^* > 1$, and different temperatures. The scattering data at 40 °C are imprecise because of the relatively small value of A_s which has rendered our data analysis approximate. (c) Log-log plots of $\bar{\Gamma}$ vs. C (g/g) at $\theta = 30°$, $C/C^* \gtrsim 1$, and different temperatures.

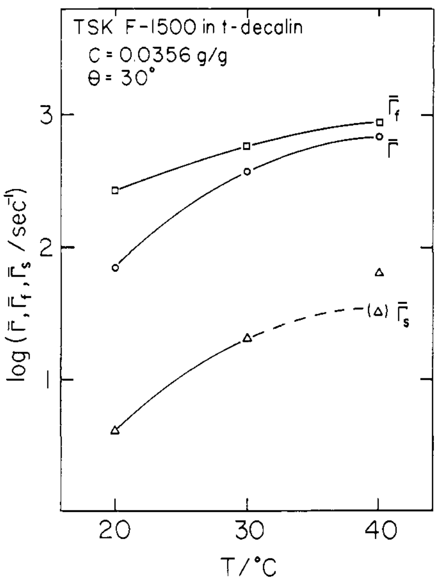

Figure 12. Log–log plot of $\bar{\Gamma}$, $\bar{\Gamma}_f$, and $\bar{\Gamma}_s$ vs. temperature for TSK F-1500 in *trans*-decalin at $C = 0.0356$ g/g and $\theta = 30°$.

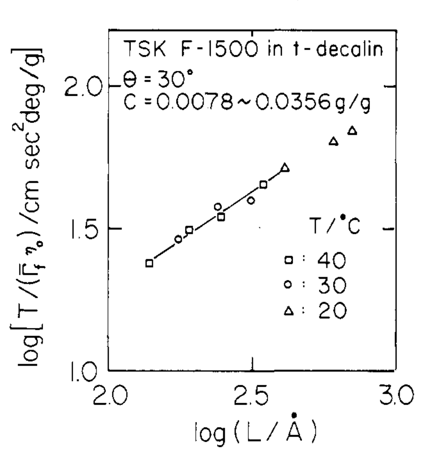

Figure 13. Log–log plot of $T/\bar{\Gamma}_f\eta_0$ vs. L at 20, 30 and 40 °C, using $\bar{\Gamma}_f$ values at $\theta = 30°$ and C from 0.00787 to 0.0356 g/g. The assumption $\bar{\Gamma}_f \sim D_g$ is not valid. Neither is $L \equiv \xi$ due to pseudogel motion only; slope (at 40°) ~ 0.68.

temperature. In the semidilute region, as $\xi_h = k_BT/6\pi\eta_0D_g$, we take $\xi_h \propto T/\eta_0\bar{\Gamma}_f$ by assuming $\bar{\Gamma}_f \sim D_g$. This assumption is not really valid as we have already shown that $\bar{\Gamma}_f$ contains information related to local internal motions. Similarly, eq 3 measured a composite characteristic length L ($\neq \xi$) in the transition region. Thus, in a log–log plot of $T/\bar{\Gamma}_f\eta_0$ vs. L as shown in Figure 13, we are making only a qualitative comparison of the relationship between ξ_h and ξ. For values at 40 °C, $\xi_h \propto \xi^\beta$ with $\beta = 0.68$. According to theory, as $\xi \propto C^q$ with $q = \nu/(1 - 3\nu) = -0.75$ for $\nu = 0.6$ and $\xi_h \propto C^{-\alpha}$ with $\alpha = \nu/(3\nu - 1) = 0.75$ for $\nu = 0.6$. Then, $\xi_h \propto \xi^{-\alpha/q}$ with $\alpha/q = -1$. We again obtained a value of 0.68 for β ($= -\alpha/q$) lower than $\beta = 1$ as predicted by theory, but the disagreement was expected. From our measurements we had $\alpha = 0.43$, $q = -0.63$, and $\beta = 0.68$. The values are internally consistent over our experimental ranges as $-\alpha/q = 0.43/0.63 = 0.68 = \beta$.

b. Relative Intensity Strength of Translational, Pseudogel, and Internal Motions. We will next report our studies on the relative intensity strength of different modes which can be observed by laser light scattering. Figure 14 shows typical plots of A_s and A_f (eq 15) as a function of temperature measured at two scattering angles (30 and 135°) for $C = 0.0356$ g/g of solution. As the radius of gyration increases with increasing temperature, both C/C^* and $K\langle r_g^2\rangle_z^{1/2}$ increase with increasing temperature. For example, as we increase the temperature from 20 to 40 °C, C/C^* changes from 2.6 to 7.3, while $K\langle r_g^2\rangle_z^{1/2}$ increases from 1.21 to 1.71 for $\theta = 30°$ and from 4.30 to 6.12 for $\theta = 135°$. In the $K\langle r_g^2\rangle_z^{1/2} - C/C^*$ plane of Figure 8, the changes are represented typically by curve a for $\theta = 30°$, $C = 0.0356$ g/g of solution, and temperatures from 20 to 40 °C. Along curve a, we are further into the pseudogel domain. The slower motions of polymer coil translation and disentanglement become less important. However, in all cases, laser light scattering was able to observe all modes of motions, indicating very strongly that we performed our studies in the transition region, not the asymptotic region which is very difficult to reach under normal experimental conditions. Figure 15a,b shows plots of R_{vv} ($\theta = 30°$) and $R_{vv,f}$ ($\theta = 30°$), $R_{vv,s}$ ($\theta = 30°$) vs. C/C^* and R_{vv} ($\theta = 135°$), $R_{vv,f}$ ($\theta = 135°$), and $R_{vv,s}$ ($\theta = 135°$) vs. C/C^*, respectively, at 30 °C. The plots are in the same spirit as those of Figure 7 of paper 2.[2] However, the nature of the subscripts s and f changes its meaning. For the slow mode, although we have identified the characteristic time at infinite dilution to be that of the translational diffusion coefficient of the entire coil, at $Kr_g \ll 1$ the slow mode in the semidilute region, nevertheless, contains information on the lifetime of polymer contact points as well as influences of the fast mode due to incomplete and approximate separation of the modes by our method of data analysis. The fast mode contains information on both local internal and pseudogel motions. At $K\langle r_g^2\rangle_z^{1/2} \sim 1.5$ and $C/C^* \sim 0.72$, $R_{vv,s}$ reaches a maximum which is responsible for the overall intensity maximum at the same C/C^*, and $R_{vv,f}$ increases until it reaches the $K_{max}\langle r_g^2\rangle_z^{1/2} = (C/C^*)^{0.61}$ line. At $\theta = 135°$ and $K\langle r_g^2\rangle_z^{1/2} = 5.5$, $R_{vv,s}$ reaches a maximum and then becomes a decreasing function of C/C^* over most of the ranges of our investigation. $R_{vv,f}$ remains a slowly increasing function in the semidilute region, and no maximum has yet been reached at $C/C^* \sim 5.3$. The overall intensity in the semidilute region remains relatively constant because of the canceling effects of $R_{vv,s}$ and $R_{vv,f}$ as a function of C/C^*.

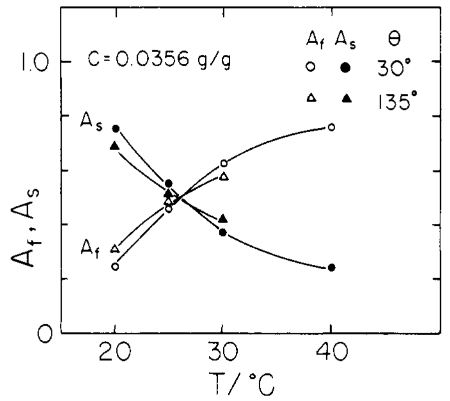

Figure 14. Plots of A_s and A_f vs. temperature at $\theta = 30$ and 130°; $C = 0.356$ g/g of solution.

Although we have made extensive studies of the static and dynamical properties of TSK F-1500 in *trans*-decalin in the semidilute region, our experimental data are still insufficient to construct a three-dimensional $K\langle r_g^2\rangle_z^{1/2} - C/C^* - A_f$ diagram. Instead, we plot constant A_f value curves in the $K\langle r_g^2\rangle_z^{1/2} - C/C^*$ plane. These values were obtained by interpolations from plots of A_f vs. $K\langle r_g^2\rangle_z^{1/2}$ at constant C/C^* and/or A_f vs. C/C^* at constant $K\langle r_g^2\rangle_z^{1/2}$. The lines in Figure 16a represent the theoretical $(C/C^*)^{0.75}$ and experimental $(C/C^*)^{0.61}$ boundaries between the domain dominated by internal motions and that dominated

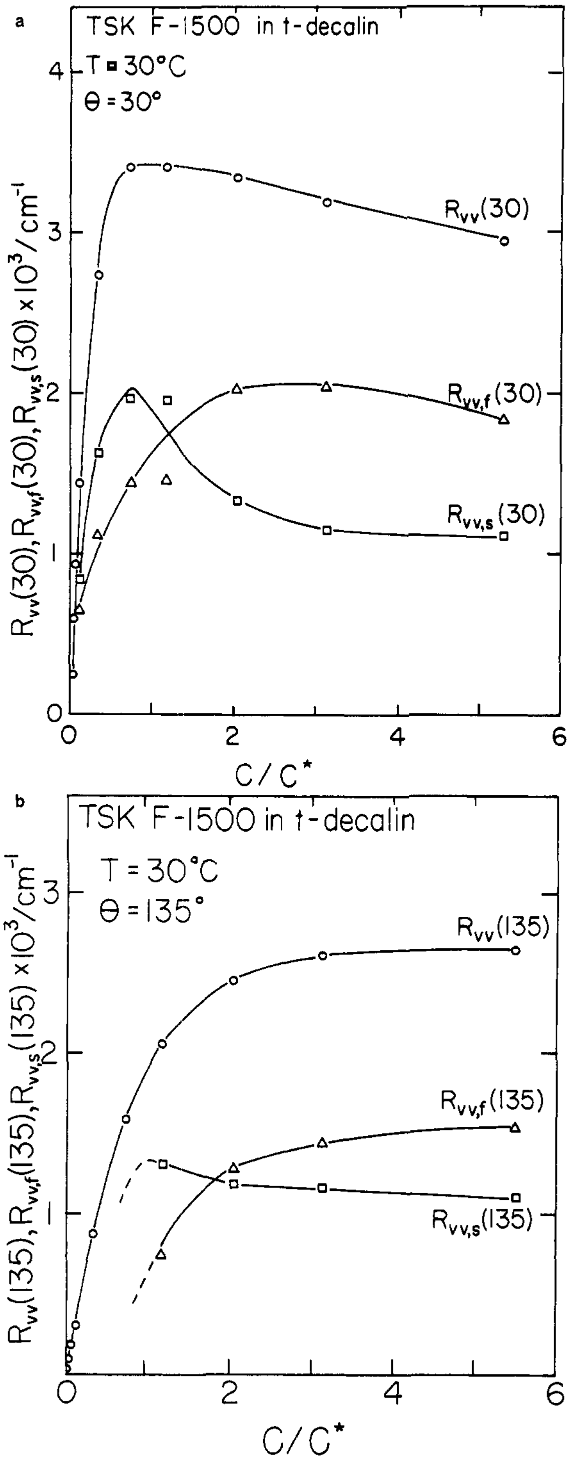

Figure 15. (a) Plots of R_{vv}, $R_{vv,f}$, and $R_{vv,s}$ vs. C/C^* for TSK F-1500 in *trans*-decalin at 30 °C and $\theta = 30°$. (b) Plots of R_{vv}, $R_{vv,f}$, and $R_{vv,s}$ vs. C/C^* for TSK F-1500 in *trans*-decalin at 30 °C and $\theta = 135°$.

by pseudogel motions. In the pseudogel domain (II), the fast pseudogel mode provides the highest contribution. For $K\langle r_g^2\rangle_z^{1/2} > 1$, the dynamical property is more gel-like with decreasing $K\langle r_g^2\rangle_z^{1/2}$ in the semidilute region, while for $K\langle r_g^2\rangle_z^{1/2} < 1$, such as the case for NBS 705 Standard, A_f increases with increasing $K\langle r_g^2\rangle_z^{1/2}$, as shown in Figure 16b.

Conclusions

By combining the results of the low molecular weight polystyrene[1,2] (NBS 705 Standard, $M_w = 1.79 \times 10^5$) with the high molecular weight polystyrene[4] (TSK F-1500, $M_w \sim 1.3 \times 10^7$) each dissolved in the same Θ solvent, *trans*-decalin, we have covered a broad experimental range of investigation, as is shown schematically in Figures 7 and 8. The asymptotic limit based on the scaling concept where simple power laws hold is quite difficult to reach under actual experimental conditions. In the semidilute region, we observed both translational motions of polymer coils and of polymer disentanglement, as well as pseudogel motions when $K\langle r_g^2\rangle_z^{1/2} < 1$, as for the case of the NBS 705 Standard polystyrene in *trans*-decalin.[1,2] When $K\langle r_g^2\rangle_z^{1/2} \sim 1$, the pseudogel motion begins to dominate with increasing concentration. For $K\langle r_g^2\rangle_z^{1/2} \gg 1$, the fast mode contains mainly information on the local internal motions at $C/C^* \sim 1$, but the pseudogel mode becomes more important at larger values of C/C^* where the state of the system again enters the pseudogel mode domain, as shown in Figure 8. We do not observe a single exponential function for all of our polymer solutions in the semidilute region. The nonexponential behavior of the dynamical structure factor is caused by several competing modes depending upon the state of the system in the $K\langle r_g^2\rangle_z^{1/2} - C/C^*$ plane. For example, larger variances in μ_2/Γ^2 at $\theta = 30°$ were observed at 20 °C than at 40 °C because of further separation of the slow and fast modes, as shown in Figure 17. In our data analysis of the transition regions, we have not been able to make complete separation of the various motions, partly because we do not have an adequate theory in interpreting $S(K,t)$ in the semidilute region

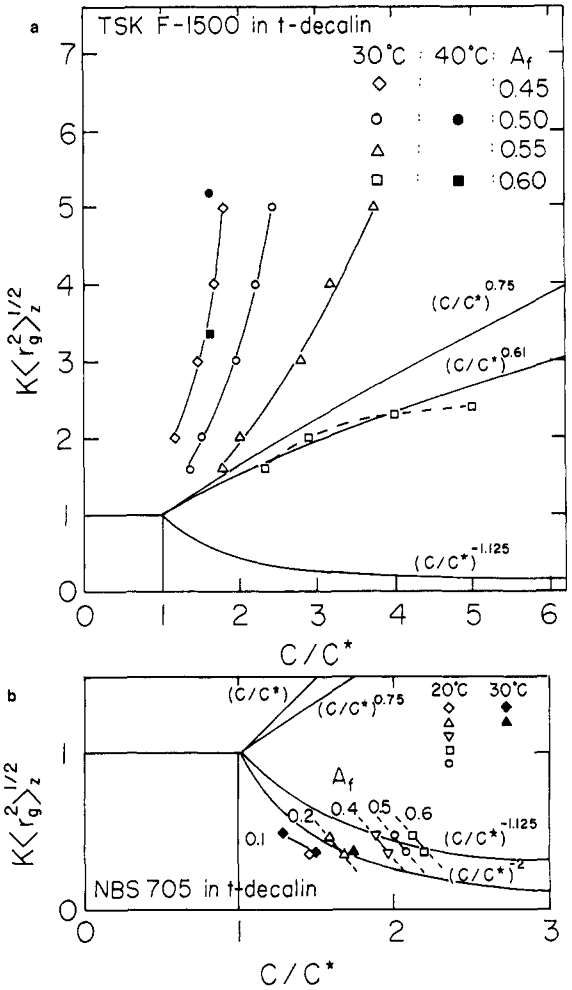

Figure 16. (a) Plots of iso-A_f curves in the $K\langle r_g^2\rangle_z^{1/2} - C/C^*$ plane for polystyrene (TSK F-1500, $M_w \sim 1.3 \times 10^7$) in *trans*-decalin at 30 °C (open symbols) and 40 °C (solid symbols). (b) Plots of iso-A_f curves in the $K\langle r_g^2\rangle_z^{1/2} - C/C^*$ plane for polystyrene (NBS 705 Standard, $M_w = 1.79 \times 10^5$) in *trans*-decalin at 20 °C (open symbols) and 30 °C (solid symbols).

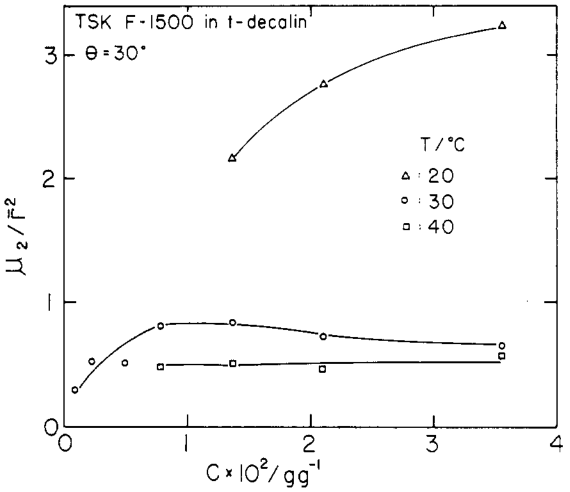

Figure 17. Plots of $\mu_2/\bar{\Gamma}^2$ vs. concentration (g/g of solution). We used $\mu_2 = A_fA_s(\Gamma_f - \Gamma_s)^2 + A_f\mu_{2f}$ and $\bar{\Gamma} = A_s\Gamma_s + A_f\Gamma_f$.

at $K\langle r_g^2\rangle_z^{1/2} > 1$ and partly because under actual experimental conditions laser light scattering can detect the different modes over large ranges in the $K\langle r_g^2\rangle_z^{1/2} - C/C^*$ plane. The boundaries specified for the various domains (I, II, and III) are not sharp, and definitive quantitative answers are available only in the asymptotic limit. Experiments which try to examine some of those limits involve a high molecular weight polymer dissolved in a good solvent, and a more complete analysis including experimental data obtained by classical means[12–20] is in progress. Further theoretical refinement in the transition regions corresponding to most actual experimental conditions should be of interest.

References and Notes

(1) T. Nose and B. Chu, *Macromolecules*, **12**, 590 (1979).
(2) B. Chu and T. Nose, *Macromolecules*, **12**, 599 (1979).
(3) Esin Gulari, Erdogan Gulari, Y. Tsunashima, and B. Chu, *J. Chem. Phys.*, **70**, 3965 (1979).
(4) T. Nose and B. Chu, *Macromolecules*, **12**, 1122 (1979).
(5) E. Dubois-Violette and P. G. de Gennes, *Physics (Long Island City, N.Y.)*, **3**, 181 (1967).
(6) M. Adam and M. Delsanti, *J. Phys. Lett.*, **38**, L271 (1977); *Macromolecules*, **10**, 1229 (1977).
(7) D. E. Koppel, *J. Chem. Phys.*, **57**, 4814 (1972).
(8) A. Ziya Akcasu and Charles C. Han, *Macromolecules*, **12**, 276 (1979).
(9) M. Nakata, S. Higashida, N. Kuwahara, S. Saeki, and M. Kaneko, *J. Chem. Phys.*, **64**, 1022 (1976).
(10) G. Weill and J. des Cloizeaux, *J. Phys. (Paris)*, **40**, 99 (1979).
(11) P. G. de Gennes, *Macromolecules*, **9**, 587, 594 (1976).
(12) L.-O. Sundelöf and B. Nyström, *Chem. Scr.*, **12**, 162 (1977).
(13) L.-O. Sundelöf and B. Nyström, *J. Polym. Sci., Polym. Lett. Ed.*, **15**, 377 (1977).
(14) B. Nyström and J. Roots, *Polymer*, **18**, 1289 (1977).
(15) B. Nyström and J. Roots, *Eur. Polym. J.*, **14**, 551 (1978).
(16) J. Roots and B. Nyström, *Eur. Polym. J.*, **14**, 773 (1978).
(17) J. Roots and B. Nyström, *J. Polym. Sci., Polym. Phys. Ed.*, **16**, 695 (1978).
(18) J. Roots and B. Nyström, *Polymer*, **20**, 148 (1979).
(19) B. Nyström, J. Roots, and R. Bergman, *Polymer*, **20**, 157 (1979).
(20) J. Roots, B. Nyström, L.-O. Sundelöf, and B. Porsch, *Polymer*, **20**, 337 (1979).

Mechanical Properties of Cast Acrylonitrile Polymers. 1. Polyacrylonitrile

Edward V. Thompson

Department of Chemical Engineering, University of Maine at Orono, Orono, Maine 04469.
Received September 11, 1979

ABSTRACT: The mechanical properties of polyacrylonitrile (PAN) cast from its monomer have been investigated, and shear creep compliance and free torsion pendulum results are reported in the 25–175 °C range for cast PAN and for PAN samples heat treated at 125 and 160 °C. Both the creep compliance and the storage modulus decrease by only slightly over one order of magnitude above the main transition region, indicating that the glass transition behavior of PAN is not analogous to that of typical amorphous polymers. Further, both the activation energies for creep and the loss modulus indicate two loss peaks, one at about 100 °C and a higher one at about 125 °C. Finally, heat treatment results in an increase in the modulus, especially above the transition region, and in the elimination of the second, higher-temperature loss peak. These results are discussed in terms of reaction of nitrile groups along the PAN backbone.

In recent years polyacrylonitrile has received widespread attention. This interest has developed principally because of the great commercial importance of polymers based on acrylonitrile, and considerable effort has been devoted to the problems of processing and fiber formation. Further, the polymer itself also has been studied extensively, not only in support of applied projects but also because of a number of interesting and sometimes unusual or unique properties. In particular, many papers have appeared dealing with color formation and decomposition and, to a lesser extent, with glass transition and multiple transition behavior and mechanical and dielectric properties. It is primarily the mechanical properties that are of interest here, but the question of heat treatment and decomposition will be seen to be of importance.

Relatively little data concerning the mechanical properties of polyacrylonitrile have appeared. Schmieder and Wolf[1] report torsion pendulum results from about −160 to 230 °C, Cotten and Schneider[2] vibrating reed results at three frequencies from about 30 to 150 °C, and Ohajima et al.[3] stretching vibrometer results from 20 to 180 °C. Further, Andrews and Okuyama[4] report creep and creep recovery studies between 70 and 160 °C and Furusho et al.[5] limited data using torsional braid analysis. The reason for the scarcity of data is mainly the difficulty in fabricating suitable test specimens, especially for creep or stress relaxation studies. The results referred to above were all obtained using either fibers or films cast from solution, since, until recently, methods for obtaining polyacrylonitrile by bulk polymerization from its monomer were

0024-9297/80/2213-0132$01.00/0